THE CHARACTERISATION OF NOTCHED 3D WOVEN COMPOSITES USING THERMO-ELASTIC STRESS ANALYSIS AND DIGITAL IMAGE CORRELATION

Paul R. Cunningham and Shuo Dai

Department of Aeronautical and Automotive Engineering, Loughborough University,
Epinal Way, Loughborough, Leicestershire LE11 3TU, United Kingdom
Email: p.cunningham@lboro.ac.uk, web page: http://www.lboro.ac.uk/departments/aae

Keywords: 3D Composites, Fatigue, Thermoelastic Stress Analysis, Digital Image Correlation.

ABSTRACT

Although adhesive bonding of fabricated composite structures would be the preferred option from a design for manufacture point of view, there will always be a need to use mechanical fastening for highly loaded regions. Fatigue behaviour and notch sensitivity are two of the main concerns for fabricated composite structures, despite the excellent performance of the material in the former regard. For 3D woven composites previous research has concentrated on the un-notched fatigue behaviour with less research focused on the notched properties. In the present work, the quasi-static and tension-tension fatigue behaviour of notched orthogonal and angle-interlock 3D woven carbon/epoxy composites are investigated. Digital image correlation was used to obtain the full-field strain distribution during the quasi-static tensile tests, and thermo-elastic stress analysis was used to characterise the damage progression during the fatigue tests. The DIC results revealed that the tensile strength of the 3D woven composites was not sensitive to notch size, with the notched tensile strength being less than 17% lower than the un-notched tensile strength. Limitations of the test machine capacity meant that the fatigue specimens were loaded at 60% of the ultimate failure stress. The specimens were cyclically loaded for 5,000,000 cycles without complete fracture, although the TSA results revealed progressive surface cracking around the notch. The orthogonal weave was found to have a larger surface damage area than the angle-interlock weave.

1 INTRODUCTION

Three-dimensional woven textile composites are favoured for their excellent damage tolerance due to the improvement in through-thickness properties and higher post-impact strength [1,2]. However, the in-plane quasi-static properties of 3D woven composites are generally lower than 2D laminates due to fibre crimping induced by the interlacing movement during the weaving process [1]. In addition, it has previously been reported that the fatigue properties of 3D woven composites tend to be lower than their 2D counterparts [3-5].

Fatigue behaviour and notch sensitivity are two very important aspects of composite structural design since there will always be a need to employ mechanical fastening in certain parts of the highly loaded regions of composite vehicle structures. Much research has concentrated on the un-notched fatigue behaviour of 3D woven composites [3, 4], with less research focused on the notched properties [6,7]. The tensile fatigue properties of 3D woven composites were found to be better than 2D woven laminates [4], but decrease with increasing content of through-thickness reinforcement [3, 5, 8]. The fatigue sensitivity and the quasi-static tensile strength of the investigated 3D interlock composites were found not to be influenced by the presence of a central hole [6, 7, 9]. Non-destructive testing techniques have previously been used to continuously monitor the fatigue damage in conventional laminated composites, such as acoustic emission [10], digital image correlation [11], and thermography [12]. However these techniques have not been used as widely to monitor the in-situ open-hole fatigue damage progression of 3D woven composites.

In this study, the open-hole quasi-static and tension-tension fatigue behaviour of two 3D weaves are investigated, one orthogonal and one angle-interlock [13]. The full-field strain distribution was

obtained via digital image correlation during the quasi-static open-hole tests, and the damage progression was characterised using thermos-elastic stress analysis during the fatigue tests.

2 EXPERIMENTAL SPECIFICATIONS

The 3D woven fabrics were manufactured from a traditional narrow fabric weave loom at M.Wright & Sons Ltd. A 1-by-1 orthogonal weave (W-1) and a through-thickness angle interlock weave (W-3) were produced and the idealised weave geometries illustrated in Figure 1 using TexGen [14].

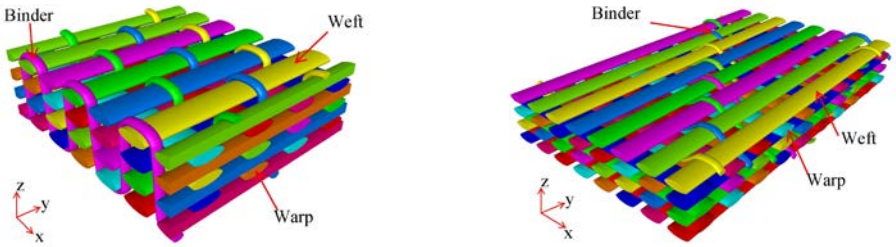

(a) (b)

Figure 1. Weave architectures (a) W-1, (b) W-3

Further details of the two weaves, including specifications for the warp, weft and binder tows, can be found in [13]. The woven fabrics were 80 mm wide, 350 mm long, and 3 mm thick, and were placed in a closed mould tool for resin transfer moulding using a Hypaject MK-III RTM system, and the resin used for the infusion was Gurit Prime 20LV with slow hardener. The final composite parts had an overall fibre volume fraction of 49.86% for W-1 and 46.01% for W-3, and a warp fibre volume fraction of 27.72% for W-1 and 25.66% for W-3. The waviness of the warp tows (defined as tow wave amplitude/unit-cell-length) was also measured on the microscopic samples and was 1.37% for W-1 and 0.55% for W-3. Detailed microscopic analysis and mechanical characterisation of the manufactured composites have been reported previously [13].

2.1 Testing

The open-hole tensile tests were carried out using an Instron 6025 testing machine with a 100 kN load cell and a LaVision DIC system to record full-field strain distribution on the surface of the specimens. All of the specimens were loaded at 2 mm/min until failure, the load and displacement data were recorded at 2 Hz, and the DIC images were recorded at 4 Hz. Based on the un-notched tensile strength of these two weaves [13], using a standard sized specimen (36mm wide) would result in a failure load of 120 kN, which is higher than the load capacity of the testing machine. Therefore the width of the samples was reduced to 25 mm. Previous literature has shown that the 3D woven composites were insensitive to the size of the notch [7], therefore five samples with a 4.1 mm diameter notch (referred to as “standard” samples) and seven samples with a 12.5 mm diameter notch (referred to as “enlarged” samples) were tested. The larger notch was used to promote failure in fatigue tests as the available fatigue machine has a load capacity of only 25 kN. In the absence of standard tests, it is only possible to perform a qualitative comparison with other research findings.

The enlarged-notched samples were used in the fatigue tests so that the maximum fatigue stress was high enough (typically 50-70% of the static strength) to induce damage to the specimen without loading for a high number of cycles. An Instron 8872 servo-hydraulic fatigue testing machine with a 25 kN load cell was used to apply a sine-wave cyclic load with a mean load of 20 kN and an amplitude of 8 kN, which resulted in the peak stress being about 63% and 61% of the static open-hole tensile strength of W-1 and W-3 respectively. A loading frequency of 20 Hz was used to minimise the non-adiabatic effect and reduce testing time [15,16]. One surface of the sample was painted in flat matt black to provide a surface with uniform emissivity of about 0.92 [17]. A FLIR Silver 450M infra-red

camera was used to record a 2 second video of the surface temperature at 383 frames/second every 10 minutes during the fatigue loading. The first video was recorded after the first 500 cycles when the temperature of the sample had stabilised. The cyclic load signal from Instron 8872 was used as a lock in signal for the thermal images in order to synchronise the thermal images with the peaks and valleys of cyclic loading. Six samples of each weave were tested for different durations to examine the damage progression at different cycles: two samples for 100,000 cycles, two samples for 500,000 cycles, one sample for 1,000,000 cycles, and one sample for 5,000,000 cycles.

4 RESULTS AND DISCUSSION

The averaged open-hole tensile strength with the two notch types, and the un-notched tensile strength which was previously published in [18], are presented in Table 1. The notch strength is the net stress calculated based on the cross-sectional area considering the hole.

Weave	ϕ (mm)	Notched Strength (MPa)	CV (%)	Un-notched Strength (MPa)	CV (%)
W-1	4.1	1145.7	4.5	1359	3.2
	12.5	1094	4.7		
W-3	4.1	1265	3.6	1281	5.8
	12.5	1202	8.0		

Table 1: Averaged quasi-static open-hole test results.

For both weaves, the enlarged samples had lower notch strength than the standard samples but differ by less than 7%. Similar results on other 3D woven orthogonal samples with 4.1 mm and 11 mm hole have been reported [7]. Although W-3 has lower un-notched tensile strength than W-1, its notched strength was higher than W-1 and showed less degradation from the un-notched tensile strength. Both W-1 samples showed about 18% reduction from the un-notched strength, while both W-3 samples showed less than 10% reduction and the standard W-3 samples showed less than 1% reduction from the un-notched strength. It has previously been observed that the broadly distributed geometrical flaws and coarse yarns cause de-bonding and reduced stress concentration around sites of failure, therefore resulting in a lower strength decrease [7,9]. The results from this work further confirmed that the stress concentration induced by a circular notch has little influence on the quasi-static tensile strength on 3D woven composites [6,7,9].

The results for the strain distribution of two typical W-1 samples at different stress levels from the DIC measurements are shown in Figure 2. Since the fibre structure of W-1 was highly orthotropic (only containing fibres in the 0º and 90º directions) and inhomogeneous (containing macroscopically distinctive resin rich regions), the strain distribution was not even and showed a strong correlation with the weave structure. The surface weave pattern was extracted and imposed on the DIC maps to emphasise the relationship between the weave pattern and strain distribution. The surface of the sample was dominated by weft tows which were perpendicular to the loading direction. Therefore a simple iso-stress assumption can be used to estimate the surface strain distribution: the region with lower stiffness will exhibit higher strain. As can be seen from Figure 2 (b) and Figure 2 (e) the resin rich channels exhibited higher strain and the centre of the weft flow region (weft region between two adjacent binders) also showed higher strain than the binder tow regions. The local longitudinal stiffness on the surface of the sample was distributed with the resin rich channels being the lowest, surface weft tow being the intermediate, and the binder region being the highest, which resulted in this strain distribution. Similar strain patterns have been reported on different types of 3D woven composites [18,19]. The strain distribution around the notch exhibited a pattern similar to the typical "butterfly" pattern in an isotropic sample. Since the resin rich channels and surface weft tow regions gave rise to a strain concentration, the higher strain regions near the notch further extended to these less stiff regions, as highlighted in the black ellipses in Figure 2 (b). At 1182 MPa (the last DIC image before fracture), the influence of the resin channels on the strain distribution was less obvious

compared with that at 340 MPa, because visually observed surface cracks in the notch region increased the apparent strain in this area. Therefore the high strain concentration areas near the notch in the strain maps (c) and (f) in Figure 2 were caused by surface cracks. The higher strain region at the upper right corner highlighted in the red ellipse in Figure 2 (c) was caused by a local manufacturing defect at the back of the sample, which later developed in to a secondary fracture site. This manufacturing defect did not affect the ultimate tensile strength of this sample since it was the warp tows in the notched region that determined the tensile strength. Similar strain distributions were found in the enlarged samples with higher strains concentrated in the resin rich channels around the notch as can be seen in Figure 2 (e). The strain concentration region near the notch also shifted at higher stress levels in Figure 2 (f) due to a visible surface cracks in these regions.

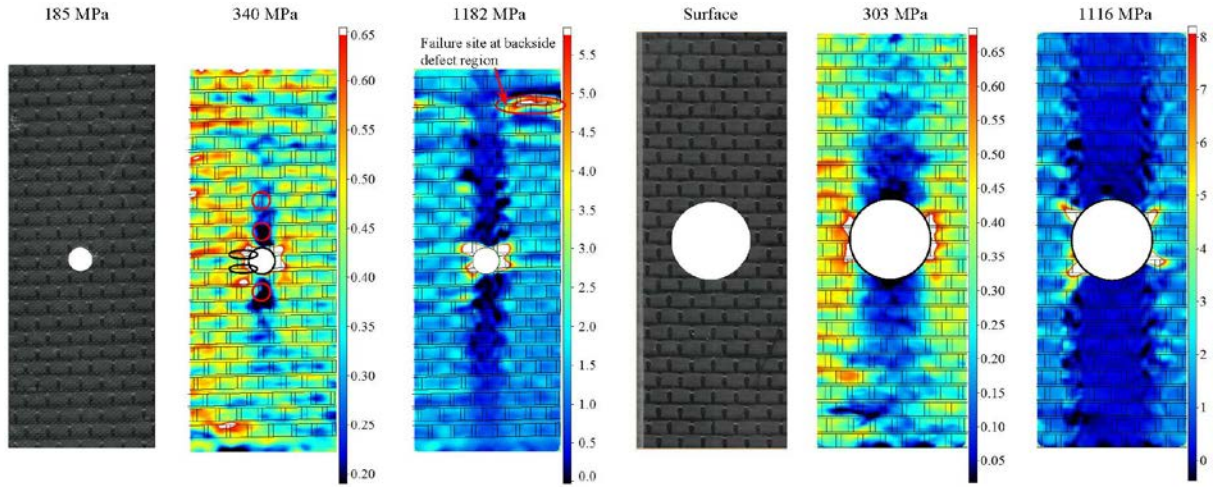

Figure 2. DIC results for the longitudinal strain (%) distribution of standard and enlarged W-1 samples at different net notch stress levels.

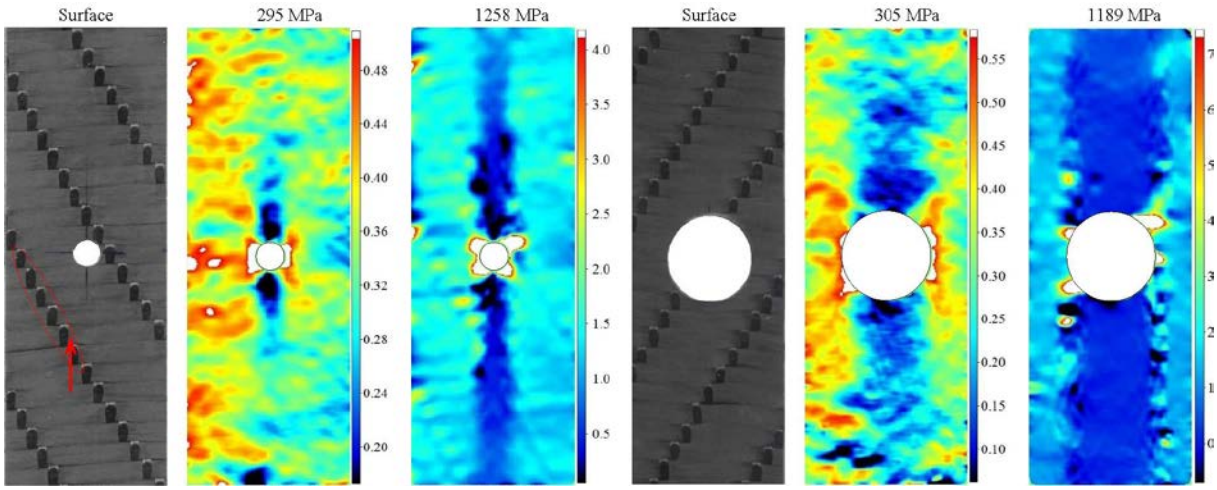

Figure 3. DIC results for the longitudinal strain (%) distribution of standard and enlarged W-3 samples at different net notch stress levels.

The longitudinal strain distribution maps of the W-3 samples are shown in Figure 3. The strain distribution of both standard and enlarged samples did not exhibit pronounced features of the weave pattern, because W-3 had smaller surface resin rich regions and was more homogeneous than W-1, resulting in a more even strain distribution. The resin rich regions around the binding points exhibited higher strain concentration at a later stage of loading as shown in Figure 3 (c). Surface cracks also developed near the hole and caused the higher strain region to shift in a diagonal direction.

In this study, the processed ΔT distribution between the peak and valley of a cycle was used to indicate fatigue damage during cyclic loading. The magnitude of ΔT (|ΔT|) distribution was plotted in this paper since it can better highlight the damage feature. Since the binder tow and the matrix have different thermal expansion coefficients and were under different stress levels, the |ΔT| distribution also reflected the surface weave patterns as shown in Figure 2 (a) and 3 (a). Similar phenomena have been observed in 2D textile composites, which showed a 0.2ºC difference between the ΔT in the resin regions and in the tow regions [12, 16]. In order to distinguish and highlight the damage from the weave pattern, a dΔT distribution map was obtained by subtracting the first ΔT map from all the other ΔT maps, which then highlighted all of the damage that occurred after the first recording.

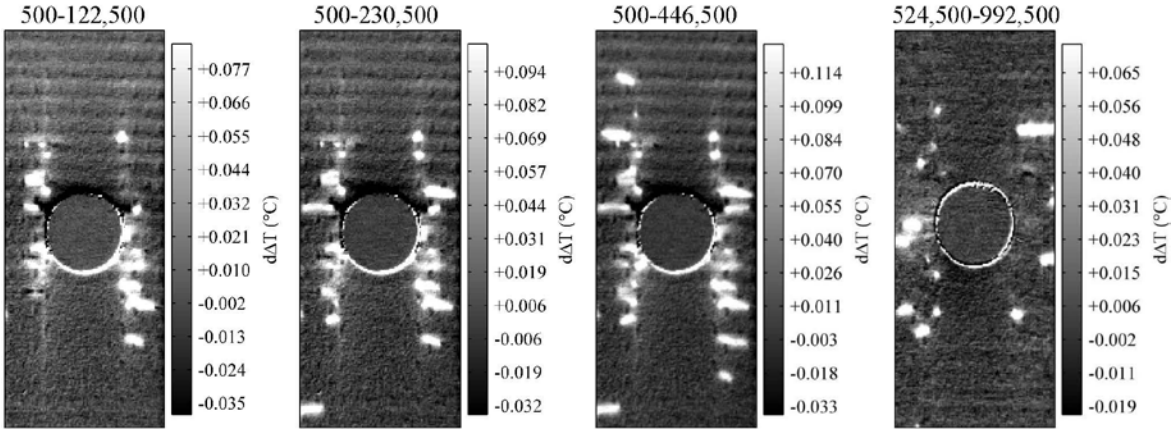

Figure 4. dΔT distribution maps of a W-1 sample during 1,000,000 cycles.

Figure 4 shows the damage that occurred between 500 and 122,500 cycles, between 500 and 230,500 cycles, between 500 and 446,500, and between 524,500 and 992,500 cycles. As can be see, most of the damage initiated within the first 122,500 cycles and propagated at a lower speed afterwards. Only a limited amount of damage occurred between 524,500 and 992,500 cycles, which indicated the damage propagation and new damage initiation process had slowed down.

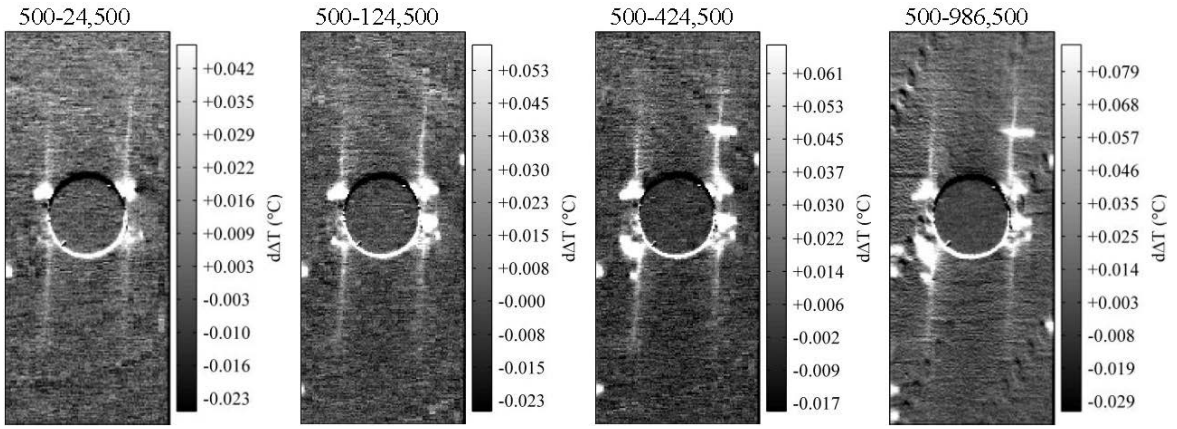

Figure 5. dΔT distribution maps of a W-3 sample during 1,000,000 cycles.

Figure 5 shows the dΔT distribution of a W-3 sample during 1,000,000 cycles. Longitudinal cracks appeared at the very beginning of loading and did not propagate through-out the entire cyclic loading process. Transverse cracks initiated from the longitudinal cracks around the notch and propagated in the weft direction. Both in-tow and between-tow matrix cracks occurred within 124,500 cycles, and one between-tow matrix crack (crack-5 in Figure 6) appeared after 196,500 cycles from the longitudinal crack about 13 mm away from the notch. In order to see the damage propagation more clearly, the length of the cracks were measured on the |ΔT| maps as plotted in Figure 6. The crack propagation clearly showed two stages: initial propagation and stabilisation. Most of the cracks except crack-5 propagated more rapidly within 100,000 cycles after initiation and stabilised after 200,000 cycles. Crack-5 initiated at about 150,000 cycles and propagated for about 300,000 cycles before slowing down. The damage initiation and progression scheme was similar in the other samples with different loading cycles.

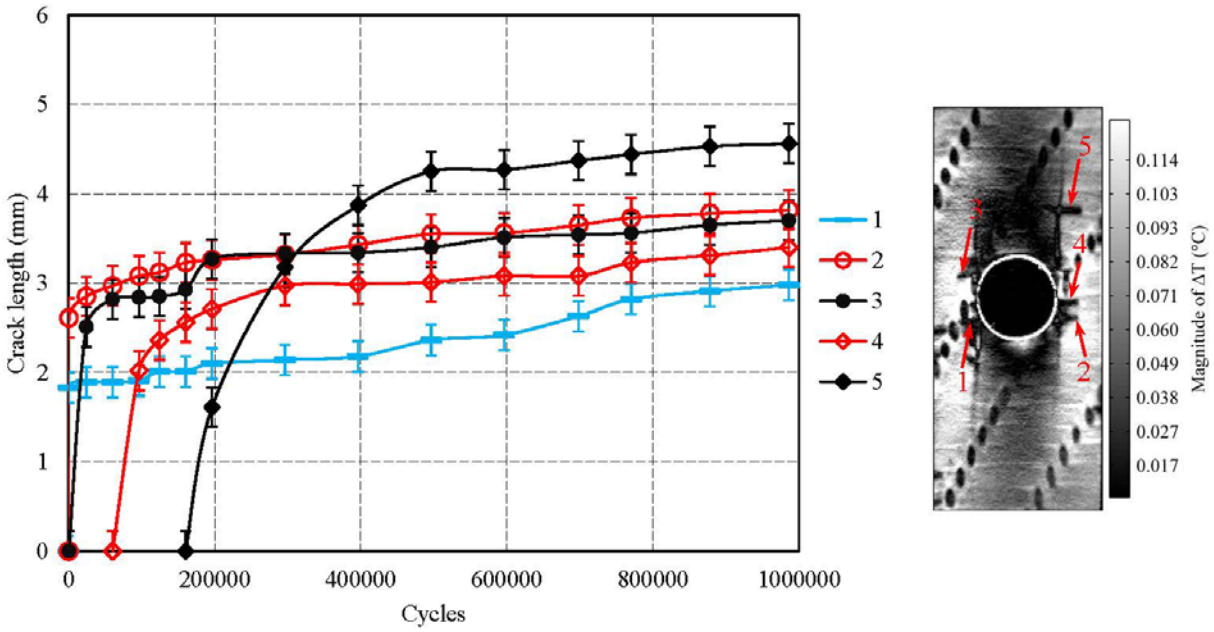

Figure 6. Crack length versus number of cycles for surface cracks on sample W-3.

The surface damage area from the dΔT maps was also extracted and the percentage of damage area over the entire sample area was obtained at each recording. Figure 7 shows the surface damage area development during fatigue loading for each sample. As can be seen, the damage growth was the fastest in the first 100,000 cycles in both weaves and gradually slowed down afterwards. Although in the first 100,000 cycles the damage area percentage of both weaves were similar, the damage area increased at a slower rate in W-3 than in W-1 after 100,000 cycles. The damage area of W-3 almost saturated after 200,000 cycles while it kept increasing in the W-1 samples. Overall, the damage area was larger in W-1 samples than in W-3 samples because W-1 had more surface binding points that induced more matrix cracking than W-3. It should be noted that the damage area percentage only indicated the surface damage not the internal damage, because the thermal camera can only detect the temperature on the sample surface.

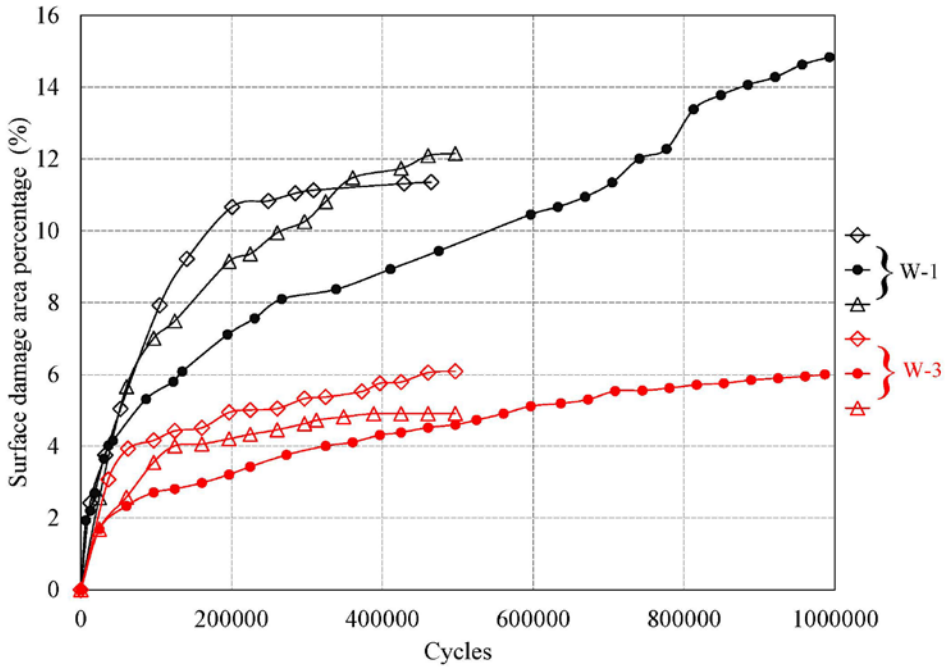

Figure 7. Percentage damage area during cyclic loading of W-1 and W-3 fatigue samples.

5 CONCLUSIONS

The following conclusions can be made following the work presented in this paper:

- The open-hole quasi-static tensile tests revealed that W-3 exhibited less reduction in its tensile strength (1-9%) than W-1 (17-20%), and using a larger notch also had little effect on the tensile strength (less than 10%), which was similar to the findings in the literature [6, 7].
- Digital image correlation maps revealed that the strain distribution of W-1 was more dependent on the weave pattern than W-3 due to its more pronounced surface resin channels.
- During cyclic loading of the open-hole fatigue samples most of the damage initiated and propagated relatively rapidly within the first 100,000 cycles and slowed down afterwards.
- Based on the temperature gradient distribution maps, W-1 showed more damage sites and more rapid damage growth than W-3.
- No complete breakage occurred to any of the samples even after 5,000,000 cycles at about 65% of the static strength, while previous research in the literature showed a 2D laminate failed within 100,000 cycles at 60% of its static strength [20].
- Overall, W-3 showed higher open-hole static strength and exhibited fewer damage sites during tension-tension fatigue open-hole tests than W-1. However, the confidence of fatigue properties would be improved with more specimens and ultimate fatigue failure would be achieved using higher stress levels.

ACKNOWLEDGEMENTS

The authors would like to gratefully acknowledge M. Wright and Sons Ltd for supporting the second author, Shuo Dai, during his PhD studies from which this work forms a part, and for supplying the material, weaving expertise and access to the loom used to manufacture the samples in this work.

REFERENCES

[1] A.P. Mouritz, *Three-dimensional (3D) fibre reinforcement for composites*, Composite reinforcements for optimum performance, Chapter 6, Woodhead Publishing, 2011.

[2] J.N. Baucom, M.A. Zikry, Low-velocity impact damage progression in woven e-glass composite systems, *Composites Part A: Applied Science and Manufacturing*, **36** (5), 2005, pp. 658–664.
[3] S. Rudov-Clark, A. P. Mouritz, Tensile fatigue properties of a 3D orthogonal woven composite, *Composites Part A: Applied Science and Manufacturing*, **39** (6), 2008, pp. 1018–1024.
[4] Y. Q. Ding, Y. Yan, R. McIlhagger, D. Brown, Comparison of the fatigue behaviour of 2D and 3D woven fabric reinforced composites, *Journal of Materials Processing Technology*, **55** (3-4), 1995, pp. 171–177.
[5] A. P. Mouritz, Tensile fatigue properties of 3D composites with through-thickness reinforcement, *Composites Science and Technology*, **68** (12), 2008, pp. 2503–2510.
[6] K. H. Tsai, C. H. Chiu, T. H. Wu, Fatigue behavior of 3D multi-layer angle interlock woven composite plates, *Composites Science and Technology* **60** (2), 2000, pp. 241–248.
[7] R. Muñoz, V. Martínez, F. Sket, C. González, J. LLorca, Mechanical behavior and failure micromechanisms of hybrid 3D woven composites in tension, *Composites Part A: Applied Science and Manufacturing* **59** (0), 2014, pp. 93–104.
[8] M. Karahan, S. V. Lomov, A. E. Bogdanovich, I. Verpoest, Fatigue tensile behavior of carbon/epoxy composite reinforced with non-crimp 3D orthogonal woven fabric, *Composites Science and Technology* **71** (16), 2011, pp. 1961–1972.
[9] B. N. Cox, M. S. Dadkhah, W. L. Morris, On the tensile failure of 3D woven composites, *Composites Part A: Applied Science and Manufacturing* **27** (6), 1996, pp. 447–458.
[10] J. Cuadra, P. A. Vanniamparambil, K. Hazeli, I. Bartoli, A. Kontsos, Damage quantification in polymer composites using a hybrid ndt approach, *Composites Science and Technology* **83** (0), 2013, pp. 11–21.
[11] W. R. Broughton, M. R. L. Gower, M. J. Lodeiro, G. D. Pilkington, R. M. Shaw, An experimental assessment of open-hole tension-tension fatigue behaviour of a GFRP laminate, *Composites Part A: Applied Science and Manufacturing* **42** (10), 2011, pp. 1310–1320.
[12] R. K. Fruehmann, J. M. Dulieu-Barton, S. Quinn, Assessment of fatigue damage evolution in woven composite materials using infra-red techniques, *Composites Science and Technology* **70** (6), 2010, pp. 937–946.
[13] S. Dai, P. R. Cunningham, S. Marshall, C. Silva, Influence of fibre architecture on the tensile, compressive and flexural behaviour of 3d woven composites, *Composites Part A: Applied Science and Manufacturing* **69** (0), 2015, pp. 195–207.
[14] University of Nottingham, TexGen URL: http://texgen.sourceforge.net/index.php/Main_Page, accessed 8 August 2013.
[15] J. M. Dulieu-Barton, Introduction to thermoelastic stress analysis, *Strain* **35** (2), 1999, pp. 35–39.
[16] R. K. Fruehmann, J. M. Dulieu-Barton, S. Quinn, On the thermoelastic response of woven composite materials, *The Journal of Strain Analysis for Engineering Design* **43** (6), 2008, pp. 435–450.
[17] A. F. Robinson, J. M. Dulieu-Barton, S. Quinn, R. L. Burguete, Paint coating characterization for thermoelastic stress analysis of metallic materials, *Measurement Science and Technology* **21** (8), 2010.
[18] D. S. Ivanov, S. V. Lomov, A. E. Bogdanovich, M. Karahan, I. Verpoest, A comparative study of tensile properties of non-crimp 3D orthogonal weave and multi-layer plain weave e-glass composites. Part II: Comprehensive experimental results, *Composites Part A: Applied Science and Manufacturing* **40** (8), 2009, pp. 1144–1157.
[19] J. P. Quinn, A. T. McIlhagger, R. McIlhagger, Examination of the failure of 3D woven composites, *Composites Part A: Applied Science and Manufacturing* **39** (2), 2008, pp. 273–283.
[20] O. J. Nixon-Pearson, S. R. Hallett, P. J. Withers, J. Rouse, Damage development in open-hole composite specimens in fatigue. Part 1: experimental investigation, *Composite Structures* **106** (0), 2013, pp. 882–889.